Correcting Distortion of Image by Image Registration

Toru Tamaki [1] Tsuyoshi Yamamura [3] Noboru Ohnishi [24]
[1]*Department of Information Engineering, Faculty of Engineering, Niigata University, Niigata 950–2181 Japan*
[2]*Center for Information Media Studies, Nagoya University, Nagoya 464–8603 Japan*
[3]*Faculty of Information Science and Technology, Aichi Prefectural University, Aichi 480–1198 Japan*
[4]*Bio-Mimetic Control Research Center, RIKEN, Nagoya 463–0003 Japan*

Abstract

We propose a method for correcting image distortion due to camera lenses by calibrating intrinsic camera parameters. The proposed method is based on image registration and doesn't require point-to-point correspondence. Parameters of three successive transformations — view change, radial distortion and illumination change — are estimated using the Gauss-Newton method. Estimating all 19 unknowns simultaneously, we introduce the implicit function theorem for calculating the Jacobian. To avoid local minima, we first estimate parameters for view change and employ coarse-to-fine minimization. Experimental results using real images demonstrate the robustness and the usefulness of the proposed method.

1. Introduction

Calibrating a camera and correcting image distortion are important processes for computer vision. Much research on calibrating extrinsic camera parameters or recovering 3D structure (for examples, see [1, 2, 3, 4]) formulate the problems without considering distortion because of simplicity. However, distortion is inevitable when we use an ordinary lens installed on an inexpensive camera; sometimes a point may be displaced more than ten pixels around the corner of the image due to distortion. Although self-calibration with a fundamental matrix[5] has been studied well recently, such studies don't take into account barrel or pin cushion distortion. Pre-calibration of intrinsic camera parameters and correction of distorted image are thus required preprocesses for such research and to produce quality images.

For researchers' convenience, some codes to calibrate intrinsic parameters have been made available through the internet (e.g., Tsai's method[6, 7] implemented by [8], or Intel CV library[9]). However, such ordinary techniques require a number of correspondences[10, 11, 12] between a point in the image and a feature point at the known three-dimensional coordinates (on a plane or on some structure like a cube or a house) to estimate parameters of transformation of the corresponding points.

When the correspondences are established manually, errors can be generated by human operation and this compromises reliability. Moreover, it takes much time and patience. For example, it is too hard to measure distortion parameters as changes in camera zooming.

An alternative procedure is to detect markers such as corners[10], circles[12], curves[13] or intersections. This can be performed by edge detection or template matching techniques that can be done on a subpixel level. However, another correspondence problem arises: When there are many feature points in a space, how do we decide which should correspond to a point on an image? It cannot be neglected as the number of the markers increases in order to improve the estimation accuracy. Even if the problem can be avoided [14], the number of points for the correspondence is still limited.

In this paper, we propose a new method for correcting image distortion due to camera lenses by calibrating intrinsic camera parameters. The proposed method establishes the correspondence between a calibration pattern (the ideal image) and a distorted picture of the pattern taken by a camera. The correspondence is based on an image registration that is often used for motion analysis. The estimation is expected to be more precise than marker detection because this method uses all points of the image rather than just using several markers. The proposed method estimates parameters of transformations of planes under perspective projection, radial distortion and spatial linear illumination change by a nonlinear optimization technique that minimizes residuals between two images.

1.1. Image registration for distortion

The basic idea is that correspondence between points is necessary for calibration, and registration can satisfy this requirement. The proposed method establishes the correspondence between an ideal calibration pattern I_1 and a distorted image I_2 of the printed pattern observed by a camera. The observation is modeled by three transformations (see Fig.1); view change $\boldsymbol{u}$, distortion $\boldsymbol{d}$, and illumination variation H. I_2 is regarded as a product generated from I_1 by applying the three functions. Using the image registration technique, the proposed method estimates the parameters of the functions by minimizing the difference between I_1 and I_2, that is, the sum of squares of intensity residuals of the two images.

The procedure of the proposed method is as follows. First, prepare calibration pattern I_1. Any digital image (taken by a digital camera, scanned photo or CG) can be used as the pattern. Second, print the pattern on a sheet of paper using a printer (we assume that the printer makes an ideal print). Third, use the camera to be calibrated to acquire an image I_2 of the printed pattern I_1. Finally, register the pattern I_1 and the observed image I_2 to determine the parameters of the functions $\boldsymbol{u}$, $\boldsymbol{d}$ and H.

Some researchers use registration to calibrate extrinsic camera parameters[1] or mosaicing[2, 15]. The problems in employing the image registration technique in a straightforward manner are that $\boldsymbol{d}$ is not a closed-form but is rather implemented by an iterative procedure, and it is difficult to obtain the gradient of $\boldsymbol{d}$ for gradient-based optimization. This is because $\boldsymbol{f}$, the inverse of $\boldsymbol{d}$, is a nonlinear function and is often used to model distortion. Although this problem occurs when distortion parameters are estimated, nothing has been found in researches of fish-eye lens mosaicing[15]. To obtain the Jacobian of $\boldsymbol{d}$, we use the implicit function theorem[16, 17]. This enables us to see the registration-based intrinsic/extrinsic parameter calibration as a unified approach including lens distortion and illumination variation.

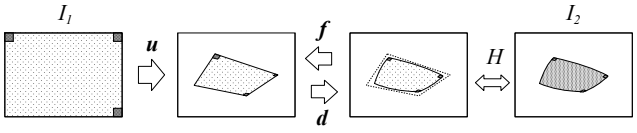

Figure 1. Observation I_2 of the calibration pattern I_1 modeled by three transformations.

Some registration-based methods have been developed [15, 18], but they require rotating a camera around a projection center for taking two (or more) pictures. In contrast, our method needs one picture from any viewpoint.

In section 2, we explain models of image transformation including view change, distortion and illumination variation. We then describe the algorithm of registration based on a nonlinear optimization in section 3. Finally, we present the experimental results in section 4.

2. Models of transformations

In this section, we describe the models of transformation between the calibration pattern I_1 and the observed image I_2. The transformation comprises three subsequent functions. The first is a change of view from pattern I_1 to a printed sheet in a 3D space, the second is the displacement from the projection of the sheet due to distortion, and the last is the illumination change that alters the intensity of the pattern.

2.1. Modeling view change

Given two images of the same planar object from different viewpoints, the relationship between them is described by a planar perspective motion model with eight parameters [2, 19]. As shown in Fig.2, I_1 and I_2 can be applied to this case for the following reason. Since I_1 is just a digital image, I_1 is a plane exactly identical to the image plane. The printed sheet is regarded as a plane transformed from the plane of I_1, and I_2 is the projection of the sheet onto the image plane having a slight displacement due to the distortion.

The model warps a point $\boldsymbol{p} = (x, y)^T$ on I_1 into the corresponding point on I_2, $\boldsymbol{p}^u = (x^u, y^u)^T$, using the function $\boldsymbol{u}$ of $\boldsymbol{\theta}^u = (\theta^u_1, \ldots, \theta^u_8)^T$ as follows[2].

$$\boldsymbol{p}^u = \boldsymbol{u}(\boldsymbol{p}, \boldsymbol{\theta}^u) = \frac{1}{\theta^u_1 x + \theta^u_2 y + 1} \begin{pmatrix} \theta^u_3 x + \theta^u_4 y + \theta^u_5 \\ \theta^u_6 x + \theta^u_7 y + \theta^u_8 \end{pmatrix} \quad (1)$$

The Jacobian of $\boldsymbol{u}$ is calculated[2] by

$$\frac{\partial \boldsymbol{u}}{\partial \boldsymbol{\theta}^u} = \begin{pmatrix} -x^2 & -xy & x & y & 1 & 0 & 0 & 0 \\ -xy & -y^2 & 0 & 0 & 0 & x & y & 1 \end{pmatrix} \quad (2)$$

2.2. Modeling distortion

The relationships between undistorted and distorted coordinates in an image are often modeled by five intrinsic camera parameters[20, 6]: the radial distortion parameters κ_1 and κ_2, the coordinates of image center $(c_x, c_y)^T$, and the aspect ratio (sometimes referred to a horizontal scale) s_x. We write these parameters as $\boldsymbol{\theta}^d = (\theta^d_1, \ldots, \theta^d_5) = (\kappa_1, \kappa_2, c_x, c_y, s_x)^T$. Although we consider only radial distortion, the following discussion can be applied when another model involving decentering distortion[21, 22] is employed.

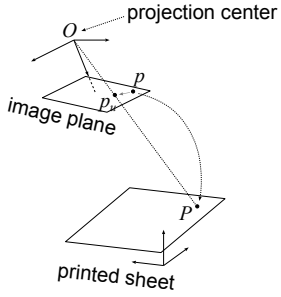

Figure 2. Relationship between I_1 and I_2.

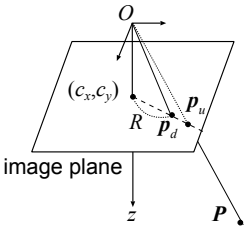

Figure 3. Distortion model

Distortion is represented with respect to the image center $(c_x, c_y)^T$. Let $\boldsymbol{p}^u = (x^u, y^u)^T$ be a point in I_2 without considering distortion, that is, $\boldsymbol{p}^u = \boldsymbol{u}(\boldsymbol{p})$; $\boldsymbol{p}^u$ is moved to $\boldsymbol{p}^d = (x^d, y^d)^T$ by radial distortion. Here we have two functions between $\boldsymbol{p}^u$ and $\boldsymbol{p}^d$.

$$\boldsymbol{p}^d = \boldsymbol{d}(\boldsymbol{p}^u, \boldsymbol{\theta}^d) \quad (3)$$

$$\boldsymbol{p}^u = \boldsymbol{f}(\boldsymbol{p}^d, \boldsymbol{\theta}^d) = \begin{pmatrix} \frac{x^d - c_x}{s_x}(1 + \kappa_1 R^2 + \kappa_2 R^4) + c_x \\ (y^d - c_y)(1 + \kappa_1 R^2 + \kappa_2 R^4) + c_y \end{pmatrix} \quad (4)$$

where $R = \sqrt{\left((x^d - c_x)/s_x\right)^2 + (y^d - c_y)^2}$. $\boldsymbol{f}$ and $\boldsymbol{d}$ are the inverse of each other, and $\boldsymbol{d}$ is not a closed-form function of $\boldsymbol{p}^u$ but is implemented by an iterative procedure[20, p.60].

In addition to the Jacobian of $\boldsymbol{u}$, the Jacobian of $\boldsymbol{d}$ is also needed for a gradient method. Here we introduce the *implicit function theorem*[16, p.144] for systems[17, p.339]. This theorem can represent the Jacobian of $\boldsymbol{d}$ as an explicit form through $\boldsymbol{f}$. Let $\boldsymbol{F}$ be a function of $\boldsymbol{q} = (\boldsymbol{p}^u, \boldsymbol{\theta}^d)$ and $\boldsymbol{p}^d$ represented by

$$\boldsymbol{F}(\boldsymbol{q}, \boldsymbol{p}^d) = \boldsymbol{p}^u - \boldsymbol{f}(\boldsymbol{p}^d, \boldsymbol{\theta}^d) \quad (5)$$

According to the definition, if $\boldsymbol{F}(\boldsymbol{q}, \boldsymbol{d}(\boldsymbol{q})) = 0$ is satisfied for $\forall \boldsymbol{p}^u$ and $\forall \boldsymbol{\theta}^d$, $\boldsymbol{p}^d = \boldsymbol{d}(\boldsymbol{q})$ is called an implicit function determined by $\boldsymbol{F}(\boldsymbol{q}, \boldsymbol{p}^d) = 0$. In our case, the condition is theoretically always satisfied because we defined $\boldsymbol{d}$ as the inverse of $\boldsymbol{f}$, and numerically Eq.(5) is almost 0 (it can be less than 10^{-10}).

According to the theorem, the Jacobian is given by the following equations.

$$\begin{aligned} \frac{\partial \boldsymbol{d}}{\partial \boldsymbol{q}} &= -\frac{\partial \boldsymbol{F}}{\partial \boldsymbol{p}^d}^{-1} \frac{\partial \boldsymbol{F}}{\partial \boldsymbol{q}} = -\frac{\partial \boldsymbol{F}}{\partial \boldsymbol{p}^d}^{-1} \left(\frac{\partial \boldsymbol{F}}{\partial \boldsymbol{p}^u} \quad \frac{\partial \boldsymbol{F}}{\partial \boldsymbol{\theta}^d} \right) \\ &= -\left(\frac{\partial \boldsymbol{F}}{\partial \boldsymbol{p}^d}^{-1} \frac{\partial \boldsymbol{F}}{\partial \boldsymbol{p}^u} \quad \frac{\partial \boldsymbol{F}}{\partial \boldsymbol{p}^d}^{-1} \frac{\partial \boldsymbol{F}}{\partial \boldsymbol{\theta}^d} \right) \end{aligned} \quad (6)$$

unless $\frac{\partial \boldsymbol{F}}{\partial \boldsymbol{p}^d}$ is singular. The Jacobian can also be decomposed into two parts as follows.

$$\frac{\partial \boldsymbol{d}}{\partial \boldsymbol{q}} = \begin{pmatrix} \frac{\partial \boldsymbol{d}}{\partial \boldsymbol{p}^u} & \frac{\partial \boldsymbol{d}}{\partial \boldsymbol{\theta}^d} \end{pmatrix} \tag{7}$$

Therefore, the second part is the desired gradient of $\boldsymbol{d}$.

$$\frac{\partial \boldsymbol{d}}{\partial \boldsymbol{\theta}^d} = -\frac{\partial \boldsymbol{F}}{\partial \boldsymbol{p}^d}^{-1} \frac{\partial \boldsymbol{F}}{\partial \boldsymbol{\theta}^d} = -\frac{\partial \boldsymbol{f}}{\partial \boldsymbol{p}^d}^{-1} \frac{\partial \boldsymbol{f}}{\partial \boldsymbol{\theta}^d} \tag{8}$$

The first part is the differential of $\boldsymbol{d}$ with respect to $\boldsymbol{p}^u = \boldsymbol{u}(\boldsymbol{p})$ (this is also used in the later formulation).

$$\frac{\partial \boldsymbol{d}}{\partial \boldsymbol{p}^u} = \frac{\partial \boldsymbol{d}}{\partial \boldsymbol{u}} = -\frac{\partial \boldsymbol{F}}{\partial \boldsymbol{p}^d}^{-1} \frac{\partial \boldsymbol{F}}{\partial \boldsymbol{p}^u} = \frac{\partial \boldsymbol{f}}{\partial \boldsymbol{p}^d}^{-1} \tag{9}$$

The derivation of elements of the Jacobian is described in [23].

2.3. Modeling illumination variation

A point $\boldsymbol{p}$ in I_1 is transformed into the point $\boldsymbol{p}^d$ in I_2 by view change and distortion. However, the intensities of the corresponding points should not be identical because gray level of the sheet on which I_1 is printed is different from the original one, and the histogram of I_2 depends on exposure of the camera, illumination of the environment, and so on.

We take the following function as a model of intensity change:

$$\begin{aligned} H(I(\boldsymbol{p}), \boldsymbol{p}, \boldsymbol{\theta}^h) = (\theta_1^h + \theta_2^h x + \theta_3^h y) I(\boldsymbol{p}) \\ + (\theta_4^h + \theta_5^h x + \theta_6^h y) \end{aligned} \tag{10}$$

where $\boldsymbol{\theta}^h = (\theta_1^h, \ldots, \theta_6^h)^T$. This model represents both the gain and bias as spatial linear functions. This is not an exact model, but it can deal with simple changes in illumination [24]. There has been an attempt to eliminate the variation in illumination[25], although it is not applicable to our case because it finds basis images from a set of images containing at least three different planes in a scene.

3. Minimization with some arrangements

In this section, we describe how to estimate the parameters of the functions $\boldsymbol{u}$, $\boldsymbol{d}$ and H. Image registration seeks to minimize the residuals r_i of intensities of the two images, I_1 and I_2.

$$r_i = I_1(\boldsymbol{p}_i) - H(I_2(\boldsymbol{p}_i^d), \boldsymbol{p}_i^d, \boldsymbol{\theta}^h) \tag{11}$$

$$\boldsymbol{p}_i^d = \boldsymbol{d}(\boldsymbol{p}_i^u, \boldsymbol{\theta}^d) \tag{12}$$

$$\boldsymbol{p}_i^u = \boldsymbol{u}(\boldsymbol{p}_i, \boldsymbol{\theta}^u) \tag{13}$$

The function to be totally minimized is the sum of squares of the residuals over the image I_1.

$$\min_{\boldsymbol{\theta}} \sum_i {r_i}^2 , \quad \boldsymbol{p}_i \in I_1 \tag{14}$$

where $\boldsymbol{\theta} = (\theta_1, \ldots, \theta_{19})^T = (\boldsymbol{\theta}^u, \boldsymbol{\theta}^d, \boldsymbol{\theta}^h)^T$.

Estimating the parameters $\boldsymbol{\theta}$, the objective function is minimized by the Gauss-Newton method, a nonlinear optimization technique[26]. The parameters are updated from some initial value by the following rule.

$$\boldsymbol{\theta} \leftarrow \boldsymbol{\theta} + \alpha\, \delta\boldsymbol{\theta} \tag{15}$$

The decent direction $\delta\boldsymbol{\theta} = (\delta\theta_1, \ldots, \delta\theta_{19})^T$ is calculated as follows[26]:

$$\delta\boldsymbol{\theta} = -(J^T J)^{-1} J^T \boldsymbol{r} \tag{16}$$

$$J = \frac{\partial \boldsymbol{r}}{\partial \boldsymbol{\theta}} \tag{17}$$

where $\boldsymbol{r} = (r_1, r_2, \ldots)^T$. This is the same as the least square formulation, that is, the system of linear equations [27] written as

$$\sum_i \sum_l \frac{\partial r_i}{\partial \theta_k} \frac{\partial r_i}{\partial \theta_l} \delta\theta_l = -\sum_i r_i \frac{\partial r_i}{\partial \theta_k} \tag{18}$$

for $k = 1, \ldots, 19$ (the number of parameters). The partial derivatives are the elements of the following Jacobian obtained by the chain rule of vector differentiation[26].

$$\frac{\partial r}{\partial \boldsymbol{\theta}} = \begin{pmatrix} \frac{\partial r}{\partial \boldsymbol{\theta}^u} & \frac{\partial r}{\partial \boldsymbol{\theta}^d} & \frac{\partial r}{\partial \boldsymbol{\theta}^h} \end{pmatrix} \tag{19}$$

$$\begin{aligned} \frac{\partial r}{\partial \boldsymbol{\theta}^u} &= \frac{\partial r}{\partial H} \left(\frac{\partial H}{\partial I_2} \frac{\partial I_2}{\partial \boldsymbol{d}} + \frac{\partial H}{\partial \boldsymbol{d}} \right) \frac{\partial \boldsymbol{d}}{\partial \boldsymbol{u}} \frac{\partial \boldsymbol{u}}{\partial \boldsymbol{\theta}^u} \\ &= -\left(\frac{\partial H}{\partial I_2} \nabla I_2(\boldsymbol{d}) + \frac{\partial H}{\partial \boldsymbol{d}} \right) \frac{\partial \boldsymbol{f}}{\partial \boldsymbol{p}^d}^{-1} \frac{\partial \boldsymbol{u}}{\partial \boldsymbol{\theta}^u} \end{aligned} \tag{20}$$

$$\begin{aligned} \frac{\partial r}{\partial \boldsymbol{\theta}^d} &= \frac{\partial r}{\partial H} \left(\frac{\partial H}{\partial I_2} \frac{\partial I_2}{\partial \boldsymbol{d}} + \frac{\partial H}{\partial \boldsymbol{d}} \right) \frac{\partial \boldsymbol{d}}{\partial \boldsymbol{\theta}^d} \\ &= \left(\frac{\partial H}{\partial I_2} \nabla I_2(\boldsymbol{d}) + \frac{\partial H}{\partial \boldsymbol{d}} \right) \frac{\partial \boldsymbol{f}}{\partial \boldsymbol{p}^d}^{-1} \frac{\partial \boldsymbol{f}}{\partial \boldsymbol{\theta}^d} \end{aligned} \tag{21}$$

$$\frac{\partial r}{\partial \boldsymbol{\theta}^h} = -\begin{pmatrix} I_2(\boldsymbol{p}^d) & x^d I_2(\boldsymbol{p}^d) & y^d I_2(\boldsymbol{p}^d) & 1 & x^d & y^d \end{pmatrix} \tag{22}$$

Once the direction is decided by solving the system of equations in Eq.(18), the step length α is optimized by line minimization[28]. The iteration of update by Eq.(15) is repeated until it converges. At each iteration, the parameters estimated in the previous iteration are used for the current Jacobian.

3.1. Interpolating pixel value

When we want to obtain the intensity of a pixel whose coordinate is not on the integer grid, as frequently occurs, we need to interpolate the intensity using the values of the pixels that are already located on the grid. For this purpose, we use the bilinear interpolation[29, p382], a simple and fast method, which interpolates the values of four neighboring pixels on a rectilinear grid.

3.2. Initial state

At the beginning of the iteration, we use the following initial value for each parameters: $\boldsymbol{\theta}^u = (0,0,1,0,0,0,1,0)^T$, $\boldsymbol{\theta}^d = (\kappa_1^0, 0, \frac{w}{2}, \frac{h}{2}, 1)^T$, and $\boldsymbol{\theta}^h = (1,0,0,0,0,0)^T$, where w and h represent the width and height of I_2, and κ_1^0 is the initial value randomly selected for κ_1 to prevent the differentials of κ_1 and κ_2 from always being 0 by initializing $\kappa_1 = \kappa_2 = 0$. We empirically choose $\kappa_1^0 \in [-10^{-7}, 10^{-7}]$.

3.3. Partial optimization

If there is a large error in estimates at the beginning of the minimization, the estimation is unstable because the number of parameters is relatively large, and $\boldsymbol{\theta}^h$ changes the intensity of the observed image.

Even though, the initial values of the estimates are always set to the values mentioned above, the minimization sometimes falls into a local minimum. To avoid the instability in the early stage of estimation, we perform the optimization for only some of the parameters, not all of them; only $\boldsymbol{\theta}^u$ is estimated, while $\boldsymbol{\theta}^d$ and $\boldsymbol{\theta}^h$ are unchanged. This is called search space decomposition[30]. There is no guarantee of convergence, but it reduces the dimension of the search space and stabilize the estimation. After the estimation of $\boldsymbol{\theta}^u$ converges, we estimate all of the parameters.

However, a good initialization is needed for a large distortion (see section 4.2).

3.4. Coarse-to-fine

To reduce computational time and to perform precise estimation even when there is a relatively large error in the initial state, we employ a strategy for shifting from a coarse resolution to a fine resolution (known as coarse-to-fine strategy). First, we use filtered blurred images with a large gaussian kernel then change the filter to a smaller one and repeat the optimization using the filtered images.

3.5. Correcting distortion

After estimating the parameters of distortion $\boldsymbol{\theta}^d$, we can correct the distortion and obtain the corrected image I'_2 by using the following relation.

$$I'_2(\boldsymbol{p}) = I_2(\boldsymbol{d}(\boldsymbol{p}, \boldsymbol{\theta}^d)) \tag{23}$$

Once we obtain the distortion parameters, we can use them for correction as long as the lens zoom is unchanged.

4. Experimental results

We conducted experiments with the proposed method using real images taken by a camera having a zoom lens. We used a scanned photograph as the calibration pattern (shown in Fig.4), printed it with a laser monochrome printer (Apple Laserwriter 16/600 PS), and then captured images of the printed sheet by a CCD video camera (Sony EVI-D30) with a video capture device (IO-DATA GV-VCP2M/PCI) of AT/PC. We placed the printed pattern in front of the camera almost parallel to the image plane. The captured image of the pattern is shown in Fig.5(a). We also took an image of a grid pattern (shown in Fig.5(c)) to help visualize the correction of distortion.

Figure 5(b) and (d) show the images corrected by Eq.(23) with the estimated parameters. In the corrected image Fig.5(d), the curved lines on the grid pattern in the distorted image are corrected to straight lines, so the proposed method works well. The computational time was about 20 minutes on a PC (866MHz CPU, GNU C++ and CLAPACK). However, the optimization had almost converged after fewer than 30 iterations.

We can see the convergence in Fig.6, which shows the sum of squares of intensity residuals of the first 25 iterations. As we mentioned in section 3.3, only $\boldsymbol{\theta}^u$ is estimated in the early stage of iteration while $\boldsymbol{\theta}^d$ and $\boldsymbol{\theta}^h$ are fixed to their initial value. After the estimation of $\boldsymbol{\theta}^u$ converges (16 iterations), the minimization using all parameters begins and converges in several iterations.

Figure 4. Calibration pattern (640×480)

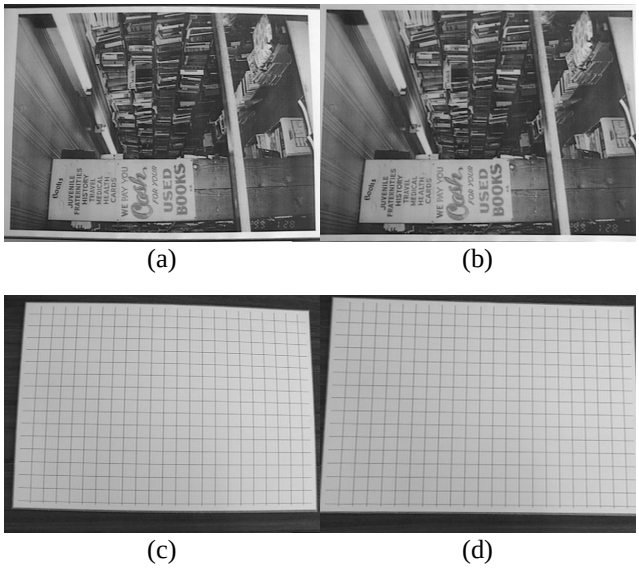

Figure 5. Experiment results of the proposed method. (a) Image of the calibration pattern taken by the camera at the widest view angle. (b) Corrected image of (a). (c) Image of the grid pattern. (d) Corrected image of (c).

4.1. Distortion parameters as changing zoom

The advantage of the proposed method is convenience for the human operator. The requirements are just a printed pattern and one captured image of it; a batch process is then called without any manual operations. This simplicity enables us to see the distortion parameter change that arises due to changing the zoom of the camera, while point correspondence-based conventional methods require an enormous number of clicking points input by a mouse. The camera that we used in the experiment above can control its zooming through a serial communication port by receiving a command[31], so that we can accurately plot the distortion parameters against zooming.

Figures 7(a) and (b) show the distortion parameters of 44 zoom settings. The horizontal axis represents the zooming (0 is the widest view angle, and the maximum zoom is 1023). We can see that the distortion parameter κ_1 monotonically decreases as the camera zooms out, while κ_2 increases and changes its sign from negative to positive. c_x, c_y and s_x are shown in Figs.7(c)(d) and (e). Apparently, c_x and s_x change and c_y stays, however, these three parameters become less precise when κ_1 (and κ_2) is small because, if there is no distortion ($\kappa_1 = \kappa_2 = 0$), c_x, c_y and s_x are indefinite.

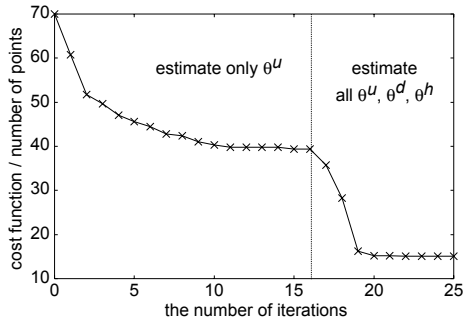

Figure 6. Convergence of the estimation. Horizontal axis is the number of iterations to update the estimates; vertical axis represents the sum of squares divided by the number of points in I_1.

Note that the horizontal axis of Fig.7 is not identical to the focal length of the camera but is just a parameter to control zooming of the lens. The zooming parameter is related to the focal length, but it doesn't mean that the parameter is linearly proportional to the focal length.

4.2. Severe distortion and convergence

Another result of correcting a distorted image is shown in Fig.8. Figure 8(a) is a grid pattern captured by another camera (Sony DXC-200A) with a wide angle lens (Sony VCL-4V10XEA). Figure 8(b) is the image corrected using the proposed method. For such severe distortion, the proposed method requires an appropriate initial state for the parameters to avoid falling into local minima. Instead of using the values in section 3.2, in this case, we decided the initial state as follows. We chose the coordinates of four corners of the pattern in the captured image and solved Eq.(1) as a system of equations with eight unknowns, then used the solution as the initial state of $\boldsymbol{\theta}^u$. We also set κ_1^0 to 1e-6; this larger positive value represents severe barrel distortion. Partial optimization is also slightly changed. We first fixed $\boldsymbol{\theta}^d$ and $\boldsymbol{\theta}^h$, then fixed $\boldsymbol{\theta}^h$, and finally estimated all parameters.

These devices seem to be ad hoc, therefore, much more sophisticated global optimization techniques should be used for large distortion. Even for small distortion, the optimization may fall into local minima because there are 19 unknowns. Nevertheless, the proposed method described in section 3 was executed 44 times to plot Fig.7 without any change or any interaction, and worked well throughout the experiment. The reason is that the distortion is relatively small (κ_1 is less than 4e-7) and the pattern occupied a large area in the captured image.

4.3. Mosaicing using corrected images

One of the applications of this method is improving mosaicing of images. Using two distorted images, mosaicing is imperfect as seen in Fig.9(a) at the corner of the original image where the displacement of distortion is severe. In contrast, the mosaic shown in Fig.9(b) composed of two images corrected by the proposed method is correctly generated. The images were taken by a digital camera (Olympus CAMEDIA C-960ZOOM).

5. Conclusions

We have proposed a new method for correcting image distortion due to camera lenses by calibrating intrinsic camera parameters without any manual operations. The proposed method is based on image registration and consists of nonlinear optimization to estimate parameters including view change, distortion, and illumination variations. Experimental results demonstrated the efficiency of the proposed method using real images. The nonlinear optimization takes some time but is fast enough to run as a batch process. We showed two applications of the proposed method: measuring distortion parameters with changes in camera zooming and image mosaicing using corrected images.

So far the results of the correction have been evaluated qualitatively because the actual intrinsic camera parameters are unknown. A quantitative evaluation of the estimates is planned for the future.

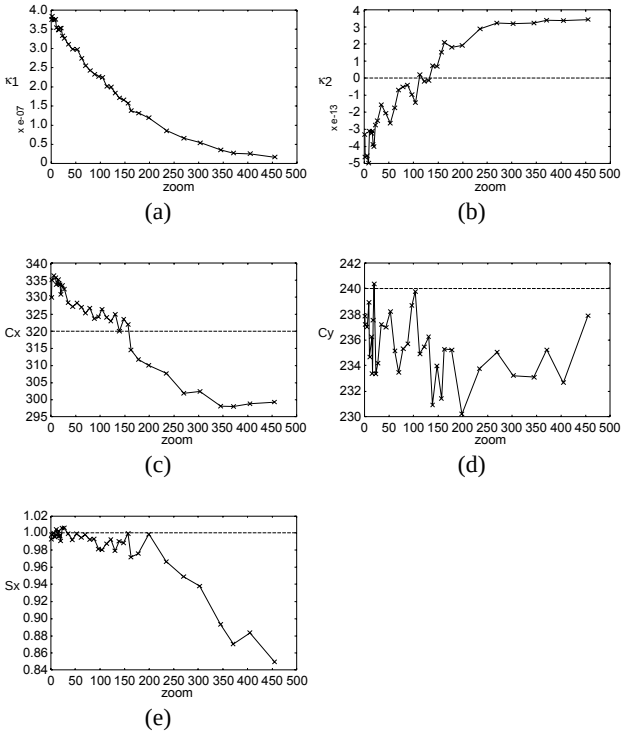

Figure 7. Change of the intrinsic parameters. (a) Distortion parameters κ_1 and (b) κ_2. (c) Image center c_x and (d) c_y. (e) Aspect ratio s_x. The horizontal axis represents the zooming of the camera; left is the wide side and right is the tele side of zoom.

6. References

[1] Y. Shibuya and I. Kumazawa, "Estimation of camera parameters and compensation of image distortion matching a priori known shape," *IEICE D-II*, vol. J83-D-II, no. 6, pp. 1460–1468, 2000. (in Japanese).

[2] H.-Y. Shum and R. Szeliski, "Systems and experiment paper: Construction of panoramic image mosaics with global and local alignment," *IJCV*, vol. 36, no. 2, pp. 101–130, 2000.

[3] T. Mukai and N. Ohnishi, "The recovery of object shape and camera motion using a sensing system with a video camera and a gyro sensor," in *Proc. of ICCV'99*, pp. 411–417, 1999.

[4] J. B. Shim, T. Mukai, and N. Ohnishi, "Improving the accuracy of 3D shape by fusing shapes obtained from optical flow," in *Proc. of CISST'99*, pp. 196–202, 1999.

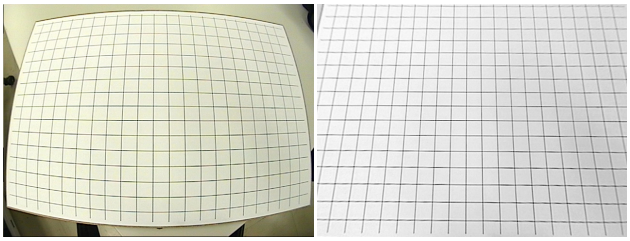

(a) (b)

Figure 8. (a) Severely distorted image (about 85 degrees horizontal and 62 degrees vertical view angles). (b) Corrected image. Estimated parameters : $\boldsymbol{\theta}^d = (1.72\text{e-}6, 1.09\text{e-}11, 305, 227, 1.026)$

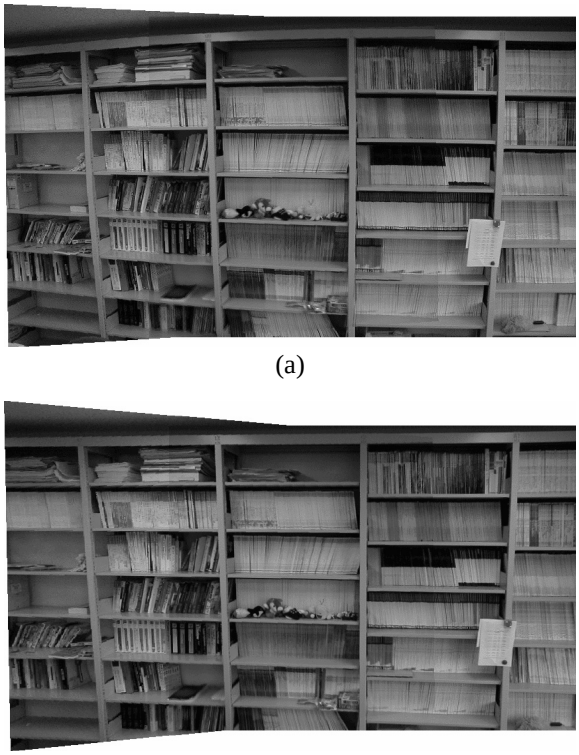

(a) (b)

Figure 9. Mosaicing of a bookshelf using (a) original images and (b) corrected images. Estimated parameters : $\boldsymbol{\theta}^d = (5.15\text{e-}7, -5.06\text{e-}13, 298, 242, 0.975)$

[5] O. D. Faugeras, ed., *Three-Dimensional Computer Vision : A Geometric Viewpoint*. MIT Press, 1993.

[6] R. Y. Tsai, "An efficient and accurate camera calibration technique for 3D machine vision," in *Proc. of CVPR'86*, pp. 364–374, 1986.

[7] R. K. Lenz and R. Y. Tsai, "Techniques for calibration of the scale factor and image center for high accuracy 3-d machine," *T-PAMI*, vol. 10, no. 5, pp. 713–720, 1988.

[8] R. Willson, "Camera calibration using Tsai's method." ftp://ftp.vislist.com/SHAREWARE/CODE/CALIBRATION /Tsai-method-v3.0b3/, 1995.

[9] G. R. Bradski and V. Pisarevsky, "Intel's computer vision library: Applications in calibration, stereo, segmentation, tracking, gesture and object recognition," in *Proc. of CVPR2000*, vol. 2, pp. 796–797, 2000. http://www.intel.com /research/mrl/research/opencv/.

[10] Z. Zhang, "A flexible new technique for camera calibration," Tech. Rep. MSR-TR-98-71, Microsoft Research, 1998. http://research.microsoft.com/~zhang/.

[11] G. P. Stein, "Lens distortion calibration using point correspondences," in *Proc. of CVPR'97*, pp. 602–608, 1997.

[12] J. Heikkilä, "Geometric camera calibration using circular control points," *T-PAMI*, vol. 22, no. 10, pp. 1066–1077, 2000.

[13] R. Swaminathan and S. K. Nayar, "Nonmetric calibration of wide-angle lenses and polycameras," *T-PAMI*, vol. 22, no. 10, pp. 1172–1178, 2000.

[14] C. Matsunaga, Y. Kanazawa, and K. Kanatani, "Optimal grid pattern for automated camera calibration using cross ratio," *IEICE Transactions on Fundamentals*, vol. E83-A, no. 10, pp. 1921–1928, 2000.

[15] Y. Xiong and K. Turkowski, "Creating image-based VR using a self-calibrating fisheye lens," in *Proc. of CVPR'97*, pp. 237–243, 1997.

[16] G. Pedrick, *A First Course in Analysis*. Springer-Verlag, 1994.

[17] M. H. Protter and C. B. Morrey, *A First Course in Real Analysis*. Springer-Verlag, 1977.

[18] H. S. Sawhney and R. Kumar, "True multi-image alignment and its application to mosaicing and lens distortion correction," *T-PAMI*, vol. 21, no. 3, pp. 235–243, 1999.

[19] R. Szeliski, "Video mosaics for virtual environment," *IEEE Computer Graphics and Applications*, vol. 16, no. 3, pp. 22–30, 1996.

[20] R. Klette, K. Schlüns, and A. Koschan, *Computer Vision Three-Dimensional Data from Images*. Singapore: Springer-Verlag, 1998.

[21] J. Weng, P. Cohen, and M. Herniou, "Camera calibration with distortion models and accuracy evaluation," *T-PAMI*, vol. 14, no. 10, pp. 965–980, 1992.

[22] C. C. Slama, ed., *Manual of Photogrammetry*. American Society of Photogrammetry, 1980.

[23] T. Tamaki, T. Yamamura, and N. Ohnishi, "A method for compensation of image distortion with image registration," *IEICE Trans. Inf. Syst.*, vol. E84-D, no. 8, pp. 990–998, 2001. http://search.ieice.org/2001/files/e000d08.htm#e84-d,8,990.

[24] M. J. Black, D. J. Fleet, and Y. Yacoob, "Robustly estimating changes in image appearance," *CVIU*, vol. 78, no. 1, pp. 8–31, 2000.

[25] P. N. Belhumeur and D. J. Kriegman, "What is the set of images of an object under all possible illumination conditions?," *IJCV*, vol. 28, no. 3, pp. 1–16, 1998.

[26] G. A. F. Seber and C. J. Wild, *Nonlinear Regression*. New York: Wiley, 1989.

[27] H. S. Sawhney and S. Ayer, "Compact representations of videos through dominant and multiple motion estimation," *T-PAMI*, vol. 18, no. 8, pp. 814–830, 1996.

[28] W. H. Press, S. A. Teukolsky, W. T. Vetterling, and B. P. Flannery, *Numerical recipes in C*. Cambridge University Press, 1992.

[29] R. Jain, R. Kasturi, and B. G. Schunck, *Machine Vision*. New York: McGraw-Hill, 1995.

[30] D. M. Gavrila and L. S. Davis, "3-D model-based tracking of humans in action: a multi-view approach," in *Proc. of ICPR'96*, pp. 73–80, 1996.

[31] Sony Co., *EVI-D30/D31 Command List*, 1998. Ver.1.21.